CRREL REPORT 98-1

Analysis of Linear and Monoclinal River Wave Solutions

Michael G. Ferrick and Nicholas J. Goodman

January 1998

Abstract: Linear dynamic wave and diffusion wave analytical solutions are obtained for a small, abrupt flow increase from an initial to a higher steady flow. Equations for the celerities of points along the wave profiles are developed from the solutions and related to the kinematic wave and dynamic wave celerities. The linear solutions are compared systematically in a series of case studies to evaluate the differences caused by inertia. These comparisons use the celerities of selected profile points, the paths of these points on the *x-t* plane, and complete profiles at selected times, indicating general agreement between the solutions. Initial diffusion wave inaccuracies persist over relatively short time and distance scales that increase with both the wave diffusion coefficient and Froude number. The nonlinear monoclinal wave solution parallels that of the linear dynamic wave but is applicable to arbitrarily large flow increases. As wave amplitude increases the monoclinal rating curve diverges from that for a linear wave, and the maximum Froude number and energy gradient along the profile increase and move toward the leading edge. A monoclinal–diffusion solution is developed for the diffusion wave equations, and dynamic wave–diffusion wave comparisons are made over a range of amplitudes with the same case studies used for linear waves. General dimensionless monoclinal–diffusion profiles exist for each depth ratio across the wave, while corresponding monoclinal wave profiles exhibit minor, case-specific Froude number dependence. Inertial effects on the monoclinal profiles occur near the leading edge, increase with the wave amplitude and Froude number, and are responsible for the differences between the dimensionless profiles.

Cover: Abrupt river wave moving downstream in the Sacandaga River (New York) near its confluence with the Hudson River. This surge was formed by a sudden flow increase of Stewarts Bridge Dam several kilometers upstream. (Photo by M. Ferrick.)

How to get copies of CRREL technical publications:

Department of Defense personnel and contractors may order reports through the Defense Technical Information Center:
DTIC-BR SUITE 0944
8725 JOHN J KINGMAN RD
FT BELVOIR VA 22060-6218
Telephone 1 800 225 3842
E-mail help@dtic.mil
msorders@dtic.mil
WWW http://www.dtic.dla.mil/

All others may order reports through the National Technical Information Service:
NTIS
5285 PORT ROYAL RD
SPRINGFIELD VA 22161
Telephone 1 703 487 4650
1 703 487 4639 (TDD for the hearing-impaired)
E-mail orders@ntis.fedworld.gov
WWW http://www.fedworld.gov/ntis/ntishome.html

A complete list of all CRREL technical publications is available from
USACRREL (CECRL-LP)
72 LYME RD
HANOVER NH 03755-1290
Telephone 1 603 646 4338
E-mail techpubs@crrel.usace.army.mil

For information on all aspects of the Cold Regions Research and Engineering Laboratory, visit our World Wide Web site:
http://www.crrel.usace.army.mil

CRREL Report 98-1

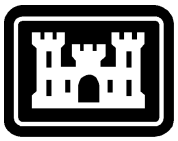

US Army Corps
of Engineers®
Cold Regions Research &
Engineering Laboratory

Analysis of Linear and Monoclinal River Wave Solutions

Michael G. Ferrick and Nicholas J. Goodman

January 1998

Prepared for
OFFICE OF THE CHIEF OF ENGINEERS

PREFACE

This report was prepared by Michael G. Ferrick, Hydrologist, and Nicholas J. Goodman, Physical Science Aid, Geological Sciences Division, Research and Engineering Directorate, U.S. Army Cold Regions Research and Engineering Laboratory, Hanover, New Hampshire. Funding for this research was provided by DA Project DT 08, *Bosnia Support*, and by CWIS Project 7VC103, *Water Resources of Cold Regions*.

The authors thank S. Daly and Dr. K. O'Neill of CRREL, K. Newyear of the University of Washington, Dr. G. Schohl of the Tennessee Valley Authority, and two anonymous reviewers for their thoughtful comments that helped to improve this manuscript. They also thank Dr. Y. Nakano of CRREL for his independent derivation of eq 19.

CONTENTS

ILLUSTRATIONS

Figure

Figure

TABLE

Table

NOMENCLATURE

B	monoclinal wave overrun unit discharge ($m^3/s \cdot m$)
$\tilde{c}$	dimensionless celerity
c_{dif}, c_{dyn}	celerity of a point on the linear diffusion wave, dynamic wave solution profiles (m/s)
c_k	kinematic wave celerity (m/s)
c_0	celerity of a disturbance in still water at the initial uniform flow depth (m/s)
c_+, c_-	dynamic wave celerity in the downstream, upstream directions (m/s)
C_*, C	dimensionless, dimensional ($m^{1/2}/s$) Chezy conveyance coefficients
D	noninertial or inertial wave diffusion coefficient (m^2/s)
E	ratio of energy gradient to bed slope gradient
F, F_0	Froude number, initial uniform flow Froude number
$F(x,t,\phi)$, F_x, F_t	implicit form of linear dynamic wave solution and its derivatives
$G(x,t,\phi)$, G_x, G_t	implicit form of linear diffusion wave solution and its derivatives
g	acceleration due to gravity (m/s)
I_0, I_1	zeroth-order, first-order modified Bessel functions of the first kind
S_f, S_0	energy and channel bed gradients
t	time (s)
U	monoclinal profile celerity (m/s)
v, v_0, v_f	flow velocity, initial uniform velocity, uniform velocity following the wave (m/s)
v_1	small increase in flow velocity from the initial uniform flow (m/s)
v_r	ratio of final to initial uniform flow velocities
v', y'	velocity derivative (1/s), depth derivative with respect to X
x_0,	distance scale, dimensionless distance in dimensionless monoclinal wave equation (m)
x	distance along the channel (m)
X	distance in a coordinate system moving at speed U with the monoclinal wave (m)
y, y_0, y_f	flow depth, initial uniform depth, and uniform depth following the wave (m)
$\tilde{y}$, $\tilde{q}$, $\tilde{q}_{steady}$	dimensionless depth, monoclinal wave unit discharge, and steady unit discharge
y_1	small increase in flow depth from the initial uniform flow (m)
y_r	ratio of final to initial uniform flow depths
y_{cr}	depth variable representing the inertia of the monoclinal wave (m)
Y	monoclinal wave depth parameter (m)
ϕ, ϕ_0, ϕ_f	dependent variable, initial and final boundary values of linear wave equations
ϕ_t, ϕ_x, ϕ_{tt}, ϕ_{xt}, ϕ_{xx}	first and second derivatives of ϕ with respect to x and t
η	parameter of linear dynamic wave equation (s)
$A(x)$, $C(x)$, H, z, α, β	parameters of the linear dynamic wave solution
C_I, C_1, C_2, C_3, C_4, C_5, C_6, C_7	parameters of the monoclinal wave solution

Analysis of Linear and Monoclinal River Wave Solutions

MICHAEL G. FERRICK AND NICHOLAS J. GOODMAN

INTRODUCTION

Much effort over several years has gone into the development and application of numerical models for unsteady river flow problems. In particular, one-dimensional numerical models that solve either the nonlinear dynamic wave or diffusion wave equations have been applied over wide ranges of river and flow conditions. Criteria for choosing a model from among these and other alternatives for given conditions have been obtained from analyses of linearized equations (Ponce and Simons 1977, Ponce et al. 1978, Menendez and Norscini 1982, Kundzewicz and Dooge 1989). Dimensionless parameters of the nonlinear equations have also been used for model selection (Woolhiser and Liggett 1967, Ferrick 1985). Several authors have treated the diffusion wave–dynamic wave modeling decision as a choice between simplicity and accuracy. However, Lighthill and Whitham (1955) argued that dynamic waves are subordinated when the flow is "well subcritical," making the characteristics of the dynamic wave system unsuitable as a basis for computation. Numerical dynamic wave and diffusion wave models cannot be readily used to resolve relative accuracy issues or to identify optimal model selection criteria.

The dynamic wave equations include flow inertia terms, and form a second-order hyperbolic system with two sets of characteristics that trace the paths of dynamic waves on the *x*-*t* plane. The diffusion wave equations neglect the inertia terms as small, resulting in a parabolic system that models a diffusing "mass wave." As the magnitude of the wave diffusion term decreases, this system approaches a zero-diffusion limit, the kinematic wave equation. This first-order hyperbolic equation has a single set of characteristics, the subcharacteristics of the dynamic wave equations, that trace the paths of kinematic waves on the *x*-*t* plane. Dynamic waves and kinematic waves are both present during unsteady river flow, and it is difficult to conceptualize their respective roles in the dynamic wave and diffusion wave models. An improved understanding of these models would be an important step toward resolution of relative accuracy and model selection questions.

Linearized forms of the dynamic wave and diffusion wave equations have been solved analytically to obtain approximate river flows (Dooge and Harley 1967, Hayami 1951). With variable coefficients treated as constants, linear solutions are strictly valid only for small flow disturbances. However, these solutions are valuable because of their common structure with corresponding nonlinear solutions. The linear dynamic wave solution is the most general and provides a standard for comparison with simpler linear solutions, but systematic comparisons have not been developed. Potential benefits include better definition of the correspondence between models, and resolution of the time and distance scales where differences are important. Relationships between dynamic wave and kinematic wave celerities and the downstream translation of linear wave profiles have not been quantified because equations for the celerity of points along these profiles are not available. Such celerity relations would clarify the roles of characteristics and subcharacteristics and provide insight into the structure of each solution.

Linear dynamic wave and diffusion wave solution comparisons cannot fully resolve the relationship between these models because large-amplitude flow increases of practical interest must be described by the nonlinear equations. This deficiency can be remedied in part by considering the monoclinal rising wave, a nonlinear dynamic wave analytical solution (Chow 1959, Henderson 1966, Whitham 1974, Hunt 1987, and Agsorn and Dooge 1991). The monoclinal wave profile is an arbitrarily large transition between low steady, uniform flow downstream and high steady flow upstream. This profile represents the balance between nonlinear wave steepening and diffusion, and has a known constant celerity that increases with wave amplitude and the kinematic wave celerity. A comparison of a corresponding nonlinear diffusion wave equation solution with the monoclinal wave would identify temporally persistent inertial effects. The monoclinal wave solution does not describe profile development nor provide the time and travel distance required to attain a steady form. However, the combination of linear wave and monoclinal wave analyses would quantify most aspects of relative dynamic wave–diffusion wave solution behavior.

The purpose of this report is to utilize analytical solutions to better understand the structure and relative behavior of the dynamic wave and diffusion wave unsteady river flow models. An abrupt flow increase between initial and final steady flows is used as an upstream boundary condition to maximize the contribution of inertia. We compare linear dynamic wave and diffusion wave solutions in a series of subcritical flow case studies. Equations for the celerity of points along each profile are derived for comparison and to explore the relationships between these profile celerities and the dynamic wave and kinematic wave celerities. This development provides the capability to trace selected profile points on the x–t plane, another means to compare the solutions. We also compare linear wave profiles to depict relative behavior through time, and give small-amplitude monoclinal profiles to assess progress toward equilibrium. Our nonlinear monoclinal wave analysis uses the same case studies as for linear waves, but considers a range of wave amplitudes. The nonlinear diffusion wave equations are solved to obtain monoclinal-diffusion profiles for comparison with the monoclinal wave. Relative steepening near the leading edge of the monoclinal profile is caused by flow inertia that persists through time. Nonlinear effects increase with wave amplitude, progressively separating monoclinal profile shapes, celerities, rating curves, and the Froude numbers and flow energy gradients along the profile from those of linear waves. Dimensionless dependent variables of the linear and monoclinal solutions provide ease of comparison, while dimensional independent variables distance and time complement physical intuition. For generality we also develop and compare fully dimensionless monoclinal and monoclinal–diffusion profiles.

LINEAR RIVER WAVE EQUATIONS

The continuity and momentum equations of unsteady flow in a wide rectangular open channel with no lateral inflow or outflow are well known (Stoker 1957, Mahmood and Yevjevich 1975):

$$\frac{\partial y}{\partial t} + v\frac{\partial y}{\partial x} + y\frac{\partial v}{\partial x} = 0 \tag{1}$$

$$\frac{\partial v}{\partial t} + v\frac{\partial v}{\partial x} + g\frac{\partial y}{\partial x} + g(S_f - S_o) = 0 \tag{2}$$

where depth y and cross-sectional average velocity v are dependent variables, S_f is the flow

energy gradient obtained from the Chezy equation with a constant conveyance coefficient, g is acceleration due to gravity, S_0 is the channel bed slope, x is distance and t is time.

Lighthill and Whitham (1955) obtained a linear form of eq 1 and 2 by substituting for y and v

$$y = y_0 + y_1$$
$$v = v_0 + v_1 \tag{3}$$

where constant y_0 and v_0 represent steady uniform flow in a channel with constant slope and resistance, and y_1 and v_1 represent small departures from that flow as

$$\frac{\partial y_1}{\partial t} + v_0 \frac{\partial y_1}{\partial x} + y_0 \frac{\partial v_1}{\partial x} = 0 \tag{4}$$

$$\frac{\partial v_1}{\partial t} + v_0 \frac{\partial v_1}{\partial x} + g \frac{\partial y_1}{\partial x} + gS_0\left(\frac{2v_1}{v_0} - \frac{y_1}{y_0}\right) = 0. \tag{5}$$

The momentum equation (eq 5) describes linear dynamic waves. If we assume that the inertia terms of eq 5 are small relative to the other terms, the momentum equation for linear diffusion waves is obtained:

$$\frac{\partial y_1}{\partial x} + S_0\left(\frac{2v_1}{v_0} - \frac{y_1}{y_0}\right) = 0. \tag{6}$$

The momentum equation for linear kinematic waves can be obtained from eq 6 by assuming the depth gradient is small relative to the bed slope and can be neglected.

Following Lighthill and Whitham (1955) we combine eq 4 and 5 to eliminate either the depth or velocity derivatives. The resulting second-order linear equations for depth or velocity are the same, and equivalent to the original system of first-order equations:

$$\phi_{tt} + 2v_0\phi_{xt} + \left(v_0 - c_0\right)(v_0 + c_0)\phi_{xx} + \frac{1}{\eta}(\phi_t + c_k\phi_x) = 0 \tag{7}$$

where the dependent variable ϕ represents either v_1 or y_1, subscripts x and t indicate differentiation with respect to those variables, $c_0 = \sqrt{gy_0}$ is the celerity of a disturbance in still water, $c_k = 3v_0/2$ is the kinematic wave celerity, and $\eta = v_0/2gS_0$. Mendoza (1995) provided an historical perspective on the development and solution of this hyperbolic equation, which we call the linear dynamic wave equation. Higher-order dynamic waves travel along two sets of characteristics described by

$$\frac{dx}{dt} = \begin{cases} v_0 + c_0 = c_+ \\ v_0 - c_0 = c_- \end{cases} \tag{8}$$

where the product of c_- and c_+, the dynamic wave celerities in the upstream (–) and downstream (+) directions for subcritical flow, appears as a coefficient in eq 7.

If the lower-order terms of eq 7 were absent, corresponding to large η, the general solution would have the form

$$\phi = \phi_1(x - c_+t) + \phi_2(x - c_-t) \tag{9}$$

with a structure totally dependent on the dynamic waves. On the other hand, if the higher-order terms were absent, corresponding to $\eta \to 0$, the general solution would have the form

$$\phi = \phi_0(x - c_kt) \tag{10}$$

depending only on lower-order kinematic waves, the subcharacteristics of eq 7. More generally both these wave types occur together, with small disturbances traveling along the characteristics and the primary mass of the flow moving along the subcharacteristics.

The same procedure used in the development of eq 7 can be repeated with eq 6 replacing eq 5, yielding

$$\phi_t + c_k \phi_x = D \phi_{xx} \tag{11}$$

where $D = c_0^2 \eta = v_0 y_0 / 2S_0$ is a noninertial diffusion coefficient. We call this parabolic advective-diffusion equation the linear diffusion wave equation. The dynamic wave celerities that appear explicitly in eq 7 depend on flow inertia, and are absent from eq 11. The Hayami (1951) solution of eq 11 is presented in Henderson (1966). Ferrick et al. (1984) developed an equation from eq 7 with the same form as eq 11 that included higher-order x-derivatives. The presence of the inertia terms resulted in an inertial diffusion coefficient that depends on the Froude number $F_0 = v_0 / c_0$:

$$D = c_0^2 \eta \left(1 - F_0^2 / 4\right). \tag{12}$$

Dooge (1973), Whitham (1974) and Menendez (1993) also obtained this inertial diffusion coefficient using different methods.

SOLUTIONS FOR LINEAR DYNAMIC AND LINEAR DIFFUSION WAVES

We will examine the linear dynamic wave and diffusion wave solutions for an instantaneous increase between steady states ϕ_0 and ϕ_f at the upstream boundary (x = 0) at t = 0. Before this increase, steady-uniform flow conditions downstream at ϕ_0 are assumed. This initial shock maximizes the importance of inertia, the difference between the dynamic wave and diffusion wave models. The solutions $\phi(x,t)$ are required for positive x and t, and for simplicity we define dimensionless $\tilde{\phi}$ as

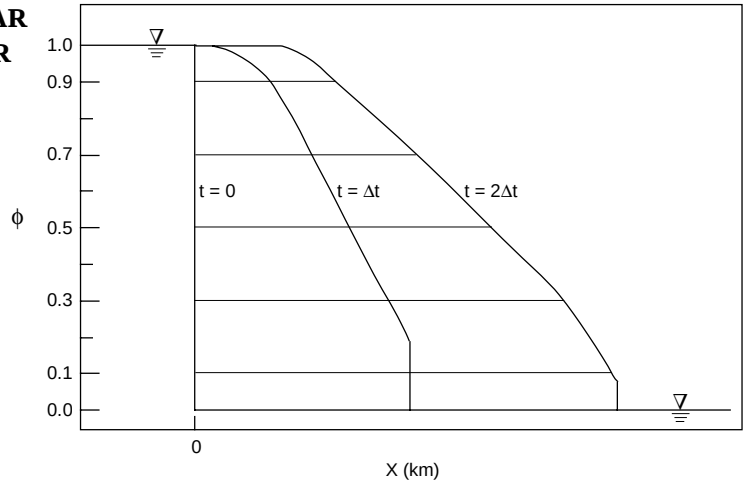

Figure 1. Initial and upstream boundary conditions of the linear equations, and dimensionless ϕ profile development with dimensional distance and time.

$$\tilde{\phi} = \frac{\phi - \phi_0}{\phi_f - \phi_0} \tag{13}$$

with $\tilde{\phi}$ = 1 at the upstream boundary and a solution interval of zero to one. In the remainder of this report we drop the tilde, but dimensionless ϕ is implied. Dimensional (x,t) and dimensionless ϕ are used in Figure 1 to depict the initial and upstream boundary conditions, and profile and shock development. Lines that trace the motion of constant ϕ profile points, and profile celerity differences between these points, related to diffusion of the profile, are indicated. Nonlinear wave steepening that opposes diffusion can cause a shock to be sustained, but it is not present here. As a result, the imposed shock attenuates and the profile separating the steady states elongates with time and distance.

The Lighthill and Whitham (1955) subcritical flow ($F_0 < 1$) solution of the linear dynamic wave equation (eq 7) for steady-uniform initial flow with a unit-step increase in ϕ at the upstream boundary is

$$\phi(x,t) = x \cdot A(x) \int_0^{t-\frac{x}{c_+}} \frac{I_1(\beta z^{1/2})}{z^{1/2}} e^{-\alpha(t-t')}\, \phi(0,t')dt' + e^{-Hx}\, \phi\left(0, t-\frac{x}{c_+}\right) \tag{14}$$

where

$$z = \left(t - t' - \frac{x}{c_+}\right)\left(t - t' - \frac{x}{c_-}\right)$$

$$\alpha = \frac{\left(1 + F_0^2\ /\ 2\right)}{2\eta}$$

$$\beta = \frac{\left(1 - F_0^2\right)^{1/2}\left(1 - F_0^2\ /\ 4\right)^{1/2}}{2\eta}$$

$$A(x) = \frac{\beta\, e^{F_0 x\ /\ 4\eta c_0}}{\left(1 - F_0^2\right) c_0}$$

$$H = \frac{1}{2\eta c_0}\left(\frac{1 - F_0\ /\ 2}{1 + F_0}\right).$$

I_1 is a first-order modified Bessel function of the first kind, and $\phi(0,t)$ is the upstream boundary condition that is equal to 0 for

$$t - \frac{x}{c_+} < 0$$

and equal to 1 otherwise.

Given x and t we can obtain ϕ with eq 14, but different dependent variable designations would be helpful for studying the solution. For example, insights could be obtained from wave profiles at specified times and from constant ϕ trajectory traces on the x-t plane. Also, it would be useful to calculate and relate the celerity of a point on the dynamic wave profile to the dynamic wave and kinematic wave celerities. To obtain these results we write eq 14 as an implicit function:

$$F(x,t,\phi) = x \cdot A(x) \int_0^{t-\frac{x}{c_+}} \frac{I_1(\beta z^{1/2})}{z^{1/2}} e^{-\alpha(t-t')}\, \phi(0,t')\, dt' + e^{-Hx}\phi\left(0, t-\frac{x}{c_+}\right) - \phi(x,t) = 0. \tag{15}$$

The dynamic wave profile celerity of a point with constant ϕ can be obtained by differentiating $F(x,t,\phi)$ and setting the result to zero as

$$c_{\mathrm{dyn}} = \frac{dx}{dt} = \frac{-F_{\mathrm{t}}}{F_{\mathrm{x}}} \tag{16}$$

where F_{x} and F_{t} are the partial derivatives of $F(x,t,\phi)$ with respect to x and t, respectively. Dividing eq 16 by the kinematic wave celerity yields dimensionless profile celerity

$$\tilde{c}_{\mathrm{dyn}} = \frac{c_{\mathrm{dyn}}}{c_{\mathrm{k}}}. \tag{17}$$

The partial derivative F_x in eq 16 can be obtained from eq 15 as

$$F_x = A(x)\left\{\int_0^{t-\frac{x}{c_+}}\left[\left(1+\frac{F_0 x}{4\eta c_0}\right)\frac{I_1(\beta z^{1/2})}{z^{1/2}}+\frac{x}{z}\frac{\partial z}{\partial x}\left(\frac{\beta}{2}I_0\left(\beta z^{1/2}\right)-\frac{I_1(\beta z^{1/2})}{z^{1/2}}\right)\right]\right.$$

$$\left. e^{-\alpha(t-t')}dt' - \frac{xC(x)}{c_+}\right\} - H\, e^{-Hx} \tag{18}$$

where

$$C(x) = \frac{\beta}{2}\, e^{-\alpha x / c_+}$$

and I_0 is a zeroth-order modified Bessel function of the first kind. Similarly, the partial derivative F_t in eq 16 can be obtained from eq 15 as

$$F_t = x \cdot A(x)\left\{C(x) + \int_0^{t-\frac{x}{c_+}}\left[-\alpha\frac{I_1(\beta z^{1/2})}{z^{1/2}}+\frac{1}{z}\frac{\partial z}{\partial t}\left(\frac{\beta}{2}I_0\left(\beta z^{1/2}\right)-\frac{I_1(\beta z^{1/2})}{z^{1/2}}\right)\right] e^{-\alpha(t-t')}dt'\right\}. \tag{19}$$

In eq 18 and 19

$$t - \frac{x}{c_+} \geq 0$$

and

$$\phi\left(0, t-\frac{x}{c_+}\right) = 1$$

are assumed.

$F(x,t,\phi)$, F_x and F_t can be computed using subroutines given by Press et al. (1992) for 10-point Gauss-Legendre integration and for polynomial approximation of modified Bessel functions. We obtain the dynamic wave profile at selected times by fixing ϕ and t and calculating the corresponding x using eq 15 and 18 in Newton's method. The half-interval method can also be used to obtain these profiles if Newton's method fails to converge. Constant ϕ trajectory traces on the x-t plane are obtained by specifying ϕ and x, and finding the corresponding t using Newton's method with eq 15 and 19.

Carslaw and Jaeger (1959) gave the solution of the linear diffusion wave equation (eq 11) subject to the initial and boundary conditions stated above, and we write it as an implicit function:

$$G(x,t,\phi) = \frac{1}{2}\left\{\operatorname{erfc}\left(\frac{x-c_k t}{(4Dt)^{1/2}}\right)+\exp\left(\frac{c_k x}{D}\right)\operatorname{erfc}\left(\frac{x+c_k t}{(4Dt)^{1/2}}\right)\right\} - \phi(x,t) = 0. \tag{20}$$

In parallel with the dynamic wave development above, for a given constant ϕ, the partial derivative of $G(x,t,\phi)$ with respect to x can be obtained from eq 20, and following simplification we obtain

$$G_x = \frac{-1}{(\pi D t)^{1/2}}\exp\left(\frac{-(x-c_k t)^2}{4Dt}\right)+\frac{c_k}{2D}\exp\left(\frac{c_k x}{D}\right)\operatorname{erfc}\left(\frac{x+c_k t}{(4Dt)^{1/2}}\right). \tag{21}$$

The partial derivative G_t can be obtained from eq 20 and simplified as

$$G_t = \frac{x}{2t(\pi D t)^{1/2}}\exp\left(\frac{-(x-c_k t)^2}{4Dt}\right). \tag{22}$$

We use the same development as above to obtain the dimensionless profile celerity for a fixed value of ϕ on the diffusion wave profile, which in simplified form is

$$\tilde{c}_{\mathrm{dif}} = \frac{-G_{\mathrm{t}} / G_{\mathrm{x}}}{c_{\mathrm{k}}} = \frac{x}{c_{\mathrm{k}} t\left[2 - c_{\mathrm{k}}\left(\frac{\pi t}{D}\right)^{1/2} \mathrm{erfc}\left(\frac{x + c_{\mathrm{k}} t}{(4Dt)^{1/2}}\right)\exp\left(\frac{(x + c_{\mathrm{k}} t)^2}{4Dt}\right)\right]}. \tag{23}$$

The forms of the linear diffusion wave and dynamic wave solutions have little apparent resemblance to each other. The kinematic wave celerity appears in each term of the diffusion wave solution (eq 20), but not in the dynamic wave solution (eq 14). The dynamic wave celerities in the downstream c_+ and upstream c_- directions both appear in z of the dynamic wave solution, and c_+ provides an upper bound on the speed of disturbances moving downstream. There is no similar restriction on disturbances traveling downstream in the diffusion wave solution. The diffusion coefficient D is an important parameter of the diffusion wave solution, while ηc_0 and η are corresponding parameters of the dynamic wave solution. The Froude number F_0 appears often in the dynamic wave solution, but is absent from the diffusion wave solution unless the inertial diffusion coefficient is used.

NONLINEAR MONOCLINAL AND MONOCLINAL–DIFFUSION WAVES

Nonlinear monoclinal wave solutions that are analogous to the linear dynamic wave and diffusion wave solutions will now be developed and compared. The term "monoclinal wave" refers to the classical solution, and "monoclinal–diffusion wave" is the solution developed after neglecting the inertia terms of momentum equation (eq 2). A monoclinal wave profile does not exist for the kinematic wave equation because diffusion is not present to balance nonlinear steepening. For completeness we summarize the monoclinal wave development of Whitham (1974), emphasizing the contribution of inertia to the solution.

We seek a solution that depends on a single variable $X = x - Ut$, where U is the constant profile celerity, and rewrite eq 1 and 2 as

$$-Uy' + vy' + yv' = \left[y(U - v)\right]' = 0 \tag{24}$$

$$(v - U)v' + gy' = gS_0 - \frac{v^2}{C_*^2 y} \tag{25}$$

respectively, where Chezy conveyance coefficients, dimensionless C_* and dimensional C, are related as

$$C_* = \frac{C}{\sqrt{g}}.$$

The first term on the left side of eq 25 follows from the inertia terms of eq 2. Integration of eq 24 yields

$$y(U - v) = B \tag{26}$$

where the constant of integration B represents a wave overrun unit discharge.

The profile celerity U is obtained from eq 26 using the flow states on either side of the wave as

$$U = \frac{v_{\mathrm{f}} y_{\mathrm{f}} - v_0 y_0}{y_{\mathrm{f}} - y_0} = \left(g\, C_*^2\, S_0\right)^{1/2}\left(\frac{y_{\mathrm{f}}^{3/2} - y_0^{3/2}}{y_{\mathrm{f}} - y_0}\right) = v_{\mathrm{f}} + \frac{v_0^2}{v_{\mathrm{f}} + v_0} \tag{27}$$

where the alternate forms are developed by eliminating either y or v using the Chezy equation. U in eq 27 is greater than v_f, and hence all velocities along the profile. With eq 27 we rewrite B in eq 26 as

$$B = y_0 y_f \left(\frac{v_f - v_0}{y_f - y_0} \right) = \left(g\, C_*^2\, S_0 \right)^{1/2} \left(\frac{y_f y_0}{y_f^{1/2} + y_0^{1/2}} \right) = \left(g\, C_*^2\, S_0 \right)^{-1} \left(\frac{v_f^2 v_0^2}{v_0 + v_f} \right). \tag{28}$$

Both U and B can be expressed in dimensionless form as

$$\frac{U}{c_k} = \frac{2}{3} \left(\frac{y_r^{3/2} - 1}{y_r - 1} \right) \tag{29}$$

$$\frac{B}{v_0 y_0} = \frac{y_r (y_r^{1/2} - 1)}{(y_r - 1)}. \tag{30}$$

These parameters increase continuously with y_r from minimums of 1 and 1/2 at $y_r = 1$, respectively, and are related to each other by a change of scale as

$$\frac{U}{c_k} = \frac{2}{3} \left(\frac{B}{v_0 y_0} + 1 \right). \tag{31}$$

In eq 29 and 30 $v_r = v_f / v_0$ can be substituted for y_r by using the Chezy equation to obtain

$$v_r = y_r^{1/2}. \tag{32}$$

Returning to the monoclinal wave equation development, we divide eq 25 by gS_0, eliminate v and v' from the inertia term using eq 24 and 26, and obtain

$$\frac{y'}{S_0} \left(1 - \frac{B^2}{g\, y^3} \right) = 1 - \frac{(v / v_0)^2}{(y / y_0)}. \tag{33}$$

Equation 26 is used again to eliminate v from eq 33, which after rearranging becomes

$$y' = \frac{S_0 \left[y^3 - \frac{1}{g\, C_*^2 S_0} \left(B - Uy \right)^2 \right]}{y^3 - y_{cr}^3} = \frac{S_0 (y - y_f)(y - y_0)(y - Y)}{y^3 - y_{cr}^3} \tag{34}$$

where

$$Y = \frac{y_0 y_f}{\left(y_f^{1/2} + y_0^{1/2} \right)^2} < y_0$$

and $y_{cr}^3 = B^2 / g$ represents the contribution of inertia.

Rewriting eq 34 in terms of convenient dimensionless variables $y_* = y / y_0$ and $\tilde{x} = x / x_0$ yields

$$\frac{dy_*}{d\tilde{x}} = \left(\frac{S_0 x_0}{y_0} \right) \frac{\left(y_* - y_r \right)\left(y_* - 1 \right)\left(y_* - \frac{Y}{y_0} \right)}{\left(y_*^3 - \left(\frac{y_{cr}}{y_0} \right)^3 \right)} \tag{35}$$

where

$$\frac{Y}{y_0} = \frac{y_r}{\left(y_r^{1/2}+1\right)^2}, \qquad \frac{y_{cr}}{y_0} = \left(\frac{F_0 y_r}{y_r^{1/2}+1}\right)^{2/3}.$$

Lighthill and Whitham (1955) deduced the monoclinal profile length as the order of y_0 / S_0. Selecting the distance scale $x_0 = y_0 / S_0$ simplifies eq 35, which then describes dimensionless monoclinal profiles that vary with y_r and F_0, and dimensionless monoclinal–diffusion profiles that depend only on y_r.

The solution of eq 34 for the monoclinal wave and monoclinal–diffusion wave profiles can be obtained by separation of variables and integration using partial fractions as

$$C_1 X + C_I = C_2 \log\left(y_f - y\right) + C_3 \log\left(y - y_0\right) + C_4 \log\left(y - Y\right)$$

$$+ C_5\left(y_f - y\right) + C_6\left(y - y_0\right) + C_7\left(y - Y\right) \tag{36}$$

where

$$C_1 = S_0\left(y_f - y_0\right)\left(y_f - Y\right)\left(y_0 - Y\right)$$

$$C_2 = \left(y_f^3 + y_{cr}^3\right)\left(y_0 - Y\right)$$

$$C_3 = -\left(y_0^3 - y_{cr}^3\right)\left(y_f - Y\right)$$

$$C_4 = \left(Y^3 - y_{cr}^3\right)\left(y_f - y_0\right)$$

$$C_5 = -y_f^2\left(y_0 - Y\right)$$

$$C_6 = -y_0^2\left(y_f - Y\right)$$

$$C_7 = Y^2\left(y_f - y_0\right).$$

C_I is a constant that results from the integration and several algebraic manipulations. We obtained C_I by specifying $X = 0$ at $y = 0.5(y_f + y_0)$. Other values of X are then obtained from eq 36 by specifying the corresponding y. The contribution of inertia in eq 36 is eliminated by setting $y_{cr} = 0$, and the monoclinal–diffusion solution results. The solution for v is obtained with y and eq 26, indicating that both monoclinal wave types have the same rating curve.

COMPARISON OF THE LINEAR SOLUTIONS

Table 1. Case studies used to compare solutions.

Case	v_0 (m/s)	y_0 (m)	S_0	η (s)	D (m²/s)	c_0 (m/s)	c_k (m/s)	c_+ (m/s)	F_0
I	0.5	1.0	0.0005	51	500	3.13	0.75	3.63	0.16
II	0.5	1.0	0.0001	255	2500	3.13	0.75	3.63	0.16
III	3.0	1.0	0.0015	102	1000	3.13	4.5	6.13	0.96
IV	3.0	3.0	0.0005	306	9000	5.42	4.5	8.42	0.55
V	1.0	3.0	0.0001	510	15000	5.42	1.5	6.42	0.18

The five cases used to compare the linear dynamic wave and diffusion wave solutions are listed in Table 1. These cases represent a wide range of conditions, with initial velocities, initial depths, and channel slopes that vary by factors of 6, 3 and 15, respectively. The corresponding variations in the parameters η, D, and F_0 by factors of 10, 30, and 6, are also large and include most of the subcritical flow range. Cases I and II represent shallow, low-velocity flows. Parameters η, D and F_0 each have relatively small values in case I. The channel

slope for case II is decreased relative to case I, while other parameters remain unchanged, corresponding to significantly increased η and D, with constant F_0. Case III is a shallow high velocity flow with channel slope and velocity increased relative to the first two cases. Parameters η and D are near those of the first case, but F_0 is at the high end of the range. Case IV represents a deeper and higher velocity flow than case I at an equal channel slope, corresponding to large η and D, with a midrange F_0. Finally, the flow in case V is deep and relatively slow with the highest η and D, and F_0 near that of cases I and II.

Dimensionless profile celerities of selected points (ϕ = 0.1, 0.3, 0.5, 0.7, 0.9) were obtained with eq 17 and 23 for dynamic waves and diffusion waves, respectively, and results for all cases are presented in Figure 2. In early time, the leading edge of the diffusion wave profile moves downstream at a celerity that initially exceeds and later is less than the dynamic wave celerity c_+. The dynamic wave and diffusion wave profile celerities of all points converge toward each other and the kinematic wave celerity with time. At the midpoint ϕ = 0.5 both profile celerities rapidly approach the kinematic wave celerity and then remain constant. Smaller ϕ profile celerities remain higher than those of larger ϕ, and diffusion continues beyond 30 km in all cases.

In case I the discrepancies between diffusion wave and dynamic wave profile celerities

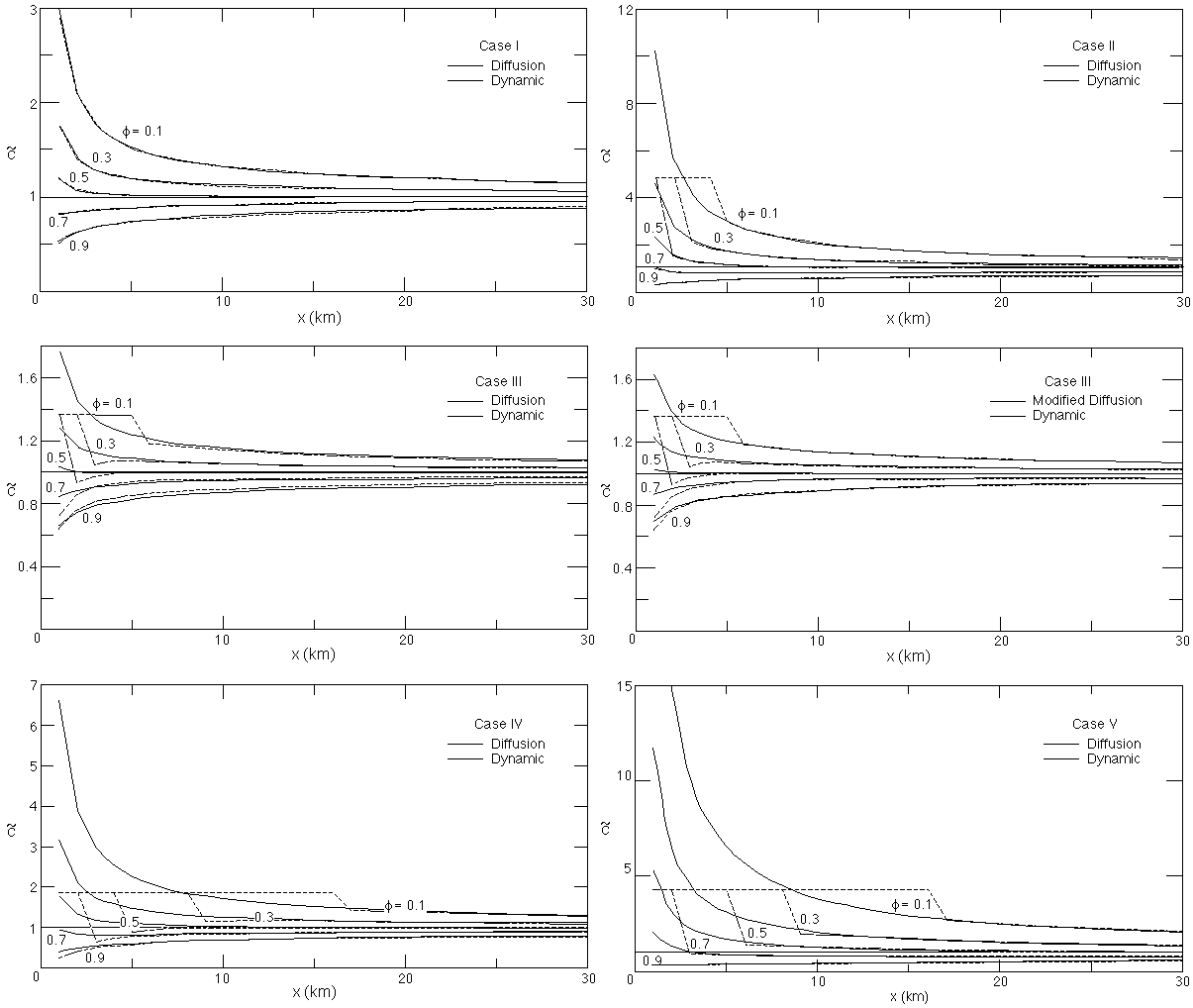

Figure 2. Dimensionless celerities of selected linear diffusion wave and dynamic wave profile points for all cases plus case III with the modified inertial diffusion coefficient. Note the changes in the celerity scale between panels.

are minor at all points after 1 km of travel distance. Initial differences between the profile celerities in case II occur as a result of the shock in the dynamic wave solution for ϕ up to 0.5, and some differences persist for 5 km downstream. Similar profile celerity disagreement is also evident in case III, but celerity convergence after shock attenuation is inexact, with a slightly larger range remaining in the diffusion wave solution. With the modified inertial diffusion coefficient (eq 12) all case III diffusion wave and dynamic wave profile celerities converge by 6 km, the distance for shock attenuation below $\phi = 0.1$. The large D in case IV causes leading edge diffusion wave profile celerities to greatly exceed the dynamic wave celerity. The shock persists for 17 km downstream, again delaying profile celerity agreement. The profile celerity change in case IV with the inertial diffusion coefficient was negligible. The celerity comparisons for case V are similar to those of case IV, with larger initial dimensionless profile celerities in both solutions, and celerity agreement at all points following shock attenuation at 17 km.

Traces on the *x*-*t* plane of selected wave profile points in Figure 3 help to visualize the effects of profile celerity differences. The time scales used for each case are related by the kinematic wave celerities given in Table 1. The dynamic wave *f* from the origin at $t = 0$, termed the dynamic forerunner by Stoker (1957), carries the initial shock downstream at a constant celerity c_+. A positive value of $F(x,t,\phi)$ immediately behind the forerunner indicates that a given ϕ is on the forerunner. The ϕ-traces that successively separate from the

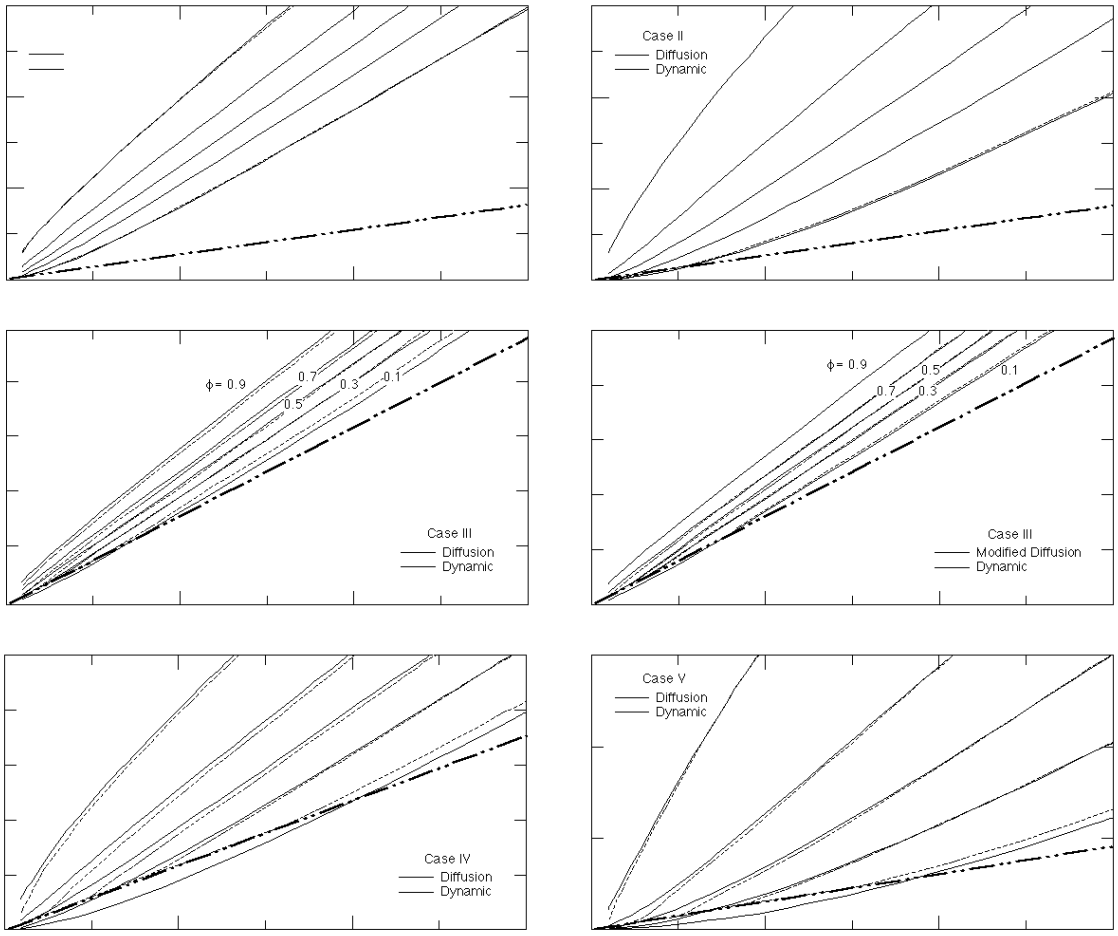

Figure 3. Traces on the x-t *plane of selected linear diffusion wave and dynamic wave profile points and the dynamic forerunner* f *for all cases plus case III with the modified inertial diffusion coefficient. Note the changes in the time scale between panels.*

dynamic forerunner indicate a progressively diminishing shock amplitude. Afterward, *f* separates from the profile and no longer contributes to the solution. Overall, the *x*-*t* traces indicate general agreement between the dynamic wave and diffusion wave solutions following attenuation of the initial shock.

The case I traces of all corresponding dynamic wave and diffusion wave profile points are essentially identical. The dynamic forerunner *f* in case I begins to separate from the profile in the first 5 km, and leads by increasing distances farther downstream. At early time in case II the diffusion profile celerity of the leading edge exceeds that of *f*, causing minor differences between the traces. These differences disappear about 5 km from the origin, and thereafter the traces of all points are identical. The forerunner and profile in case II progressively separate beyond 10 km from the origin. The high F_0 in case III reduces the rate of spread of the dynamic profile, causing the diffusion traces of the front half to lead and of the back half to lag the dynamic traces, and these trends persist. With the inertial diffusion coefficient the traces in case III agree closely beyond 8 km, and the profile progressively separates from *f* beyond 15 km. In case IV a shock amplitude of 0.1 is carried by the forerunner for 16 km, with *f* separating from the profile beyond 25 km. Excess profile spreading in the diffusion solution, caused by initial celerity differences and high diffusion coefficient, persists throughout and was not greatly improved by the inertial diffusion coefficient. The case V dynamic wave and diffusion wave traces compare similarly to those of case IV, except that differences higher on the profile do not persist.

We can compare dynamic wave and diffusion wave profiles through time on a single figure by using a moving *x*-coordinate system with origin at $\phi = 0.5$. Comparisons of these origin *x*-values through time (x_{dyn}, x_{dif}) are given in Figure 4. The origin traces of the dynamic wave model were similar for cases with the same kinematic wave celerity. The absolute value of the difference in origin position between the dynamic wave and diffusion wave models was al-

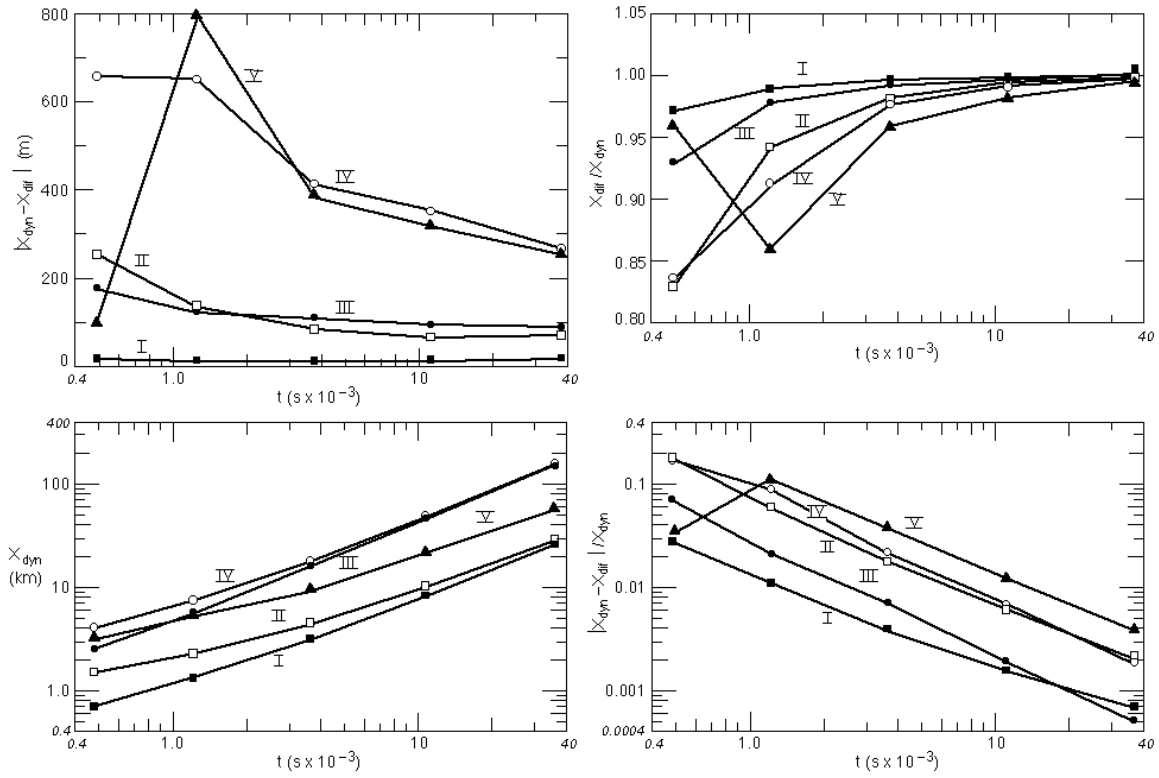

Figure 4. Comparison between origin positions of the moving coordinate system in the linear diffusion wave (x_{dif}) and dynamic wave (x_{dyn}) models for all cases.

ways less than 800 m, and diminished to less than 4 % of x_{dyn} after 1 hour. The ratio of these origin positions rapidly approached 1 from below in all cases. Larger diffusion coefficients correspond to larger absolute differences in origin position early and generally larger ratio differences from 1.

Dynamic wave and diffusion wave profiles at selected times are compared in the moving coordinate system in Figure 5. The dynamic wave solution includes the initial shock on the forerunner. At early time the leading edge of the diffusion profile always precedes that of the dynamic profile by a distance that increases with D or η and the Froude number. The profiles in case I rapidly converge and are nearly identical after 1200 s. In case II the shock front is preserved for a longer time, and the profiles converge by 10,800 s. With high F_0 in case III the profiles tend to converge after the shock diminishes, but the dynamic wave profile retains more steepness than the diffusion wave profile. Case III profiles with the inertial diffusion coefficient are nearly identical after 3600 s. In case IV the shock persists for a longer time, and profile convergence requires more than 10,800 s. The minor differences in profile steepness remaining at large times can be minimized with the inertial diffusion coefficient. The case V profile comparisons are similar to those of case IV, but with a low Froude number the inertial diffusion coefficient is not needed for agreement at large times. Monoclinal wave profiles of

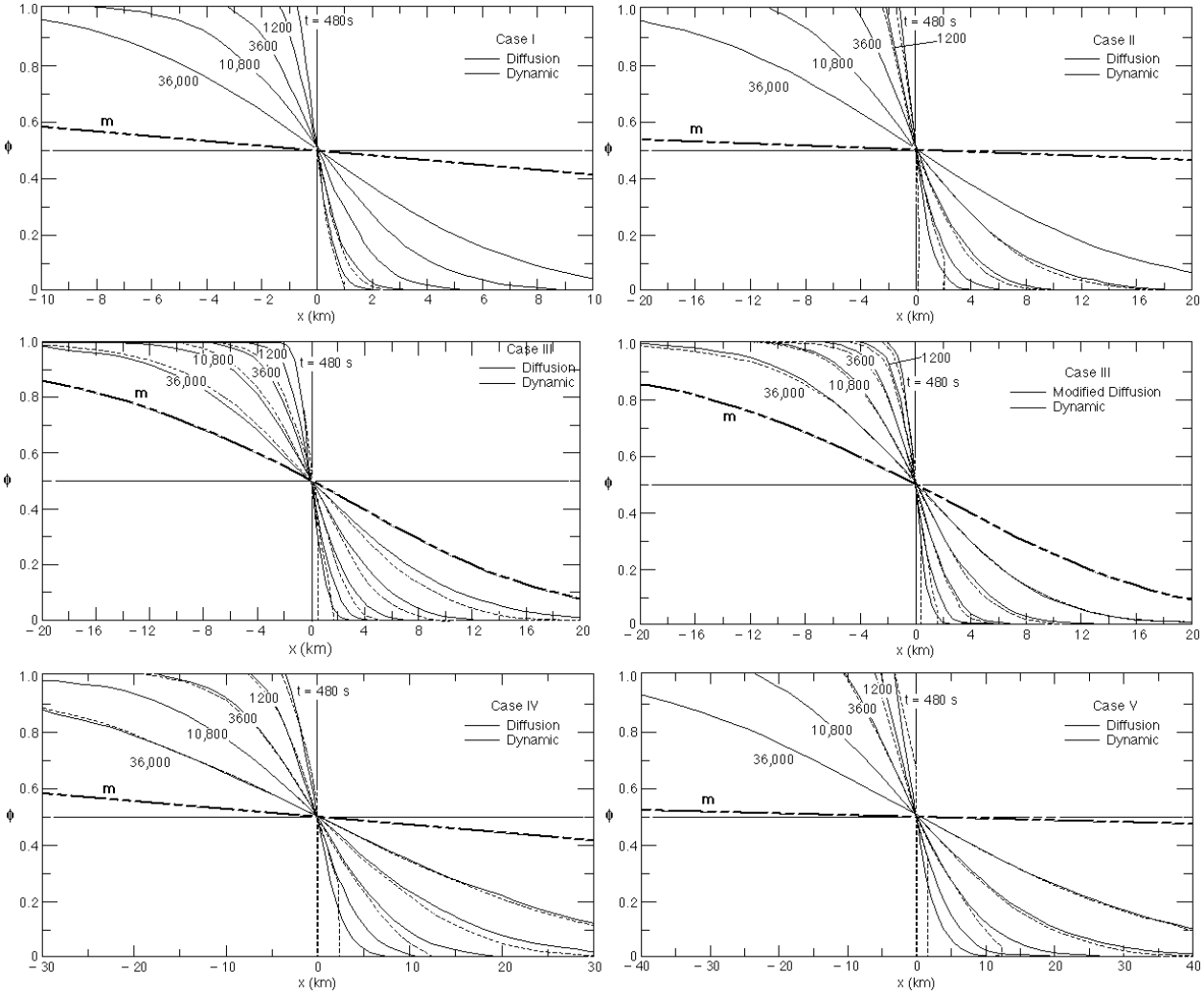

Figure 5. Linear diffusion wave and dynamic wave profiles and small-amplitude monoclinal wave profile m *for all cases plus case III with the modified inertial diffusion coefficient. Note the changes in the distance scale between panels.*

amplitude $0.1y_0$, representing fully diffused linear wave profiles at large times, are also given for each case in Figure 5. The most prominent feature of these solutions is the low profile slope, and the extended time indicated for the linear wave to attain this profile. Only the higher Froude number linear profiles at 36,000 s even approach the small-amplitude monoclinal profiles.

ANALYSIS OF THE MONOCLINAL SOLUTIONS

The numerator of the depth gradient in eq 34 does not change sign along the profile, but a sign change in the denominator can result from the presence of inertia. This sign change indicates a monoclinal wave profile that turns back upstream, becomes unstable, and forms a shock. In contrast, the monoclinal–diffusion profile cannot become unstable because y_{cr} is not present. Initial monoclinal wave instability occurs at the toe of the profile when the denominator goes to zero, and

$$y = y_0 = y_{cr}\left(\frac{B^2}{g}\right)^{1/3}. \tag{37}$$

Following Hunt (1987) we evaluate the stability limit eq 37 using eq 28, and after some algebra, the depth ratio across the wave y_r is obtained as a function of F_0

$$y_r = \left[-\frac{1}{2}+\left(\frac{1}{4}+F_0\right)^{1/2}\right]^{-2}. \tag{38}$$

The depth ratio range of stable monoclinal wave profiles decreases as Froude number increases toward 2. Conversely F_0 can be obtained as a function of y_r with eq 35 as

$$F_0 = \frac{\left(y_r^{1/2}+1\right)}{y_r}. \tag{39}$$

The stability limit in eq 37, evaluated using eq 26, yields $U = v_0+c_0$ as the maximum profile celerity prior to instability. The range of stable profile celerities, bounded below by the celerity of lower-order kinematic waves and bounded above by the celerity of higher-order dynamic waves, can be written in dimensionless form as

$$1 < \frac{U}{c_k} < \frac{2}{3}\left[1+\frac{1}{F_0}\right]. \tag{40}$$

Dimensionless profile celerity and overrun discharge given in Figure 6 increase continuously with wave amplitude from lower limits of 1 and 0.5, respectively, at $y_r = y_f / y_0 = 1$. The upper limits are indicated for selected values of F_0 by dots that follow from eq 40.

The difference between the monoclinal and monoclinal–diffusion solutions can be parameterized by considering the bracketed term in eq 33 rewritten using dimensionless variables

$$1-\frac{B^2}{gy^3} = 1-\left(\frac{y_{cr}}{y}\right)^3 = 1-\frac{\left(\frac{F_0 y_r}{y_r^{1/2}+1}\right)^2}{\left[(y_r-1)\tilde{y}+1\right]^3} \tag{41}$$

where dimensionless depth $\tilde{y}$, defined analogously to $\tilde{\phi}$ in eq 13, varies between 0 and 1.

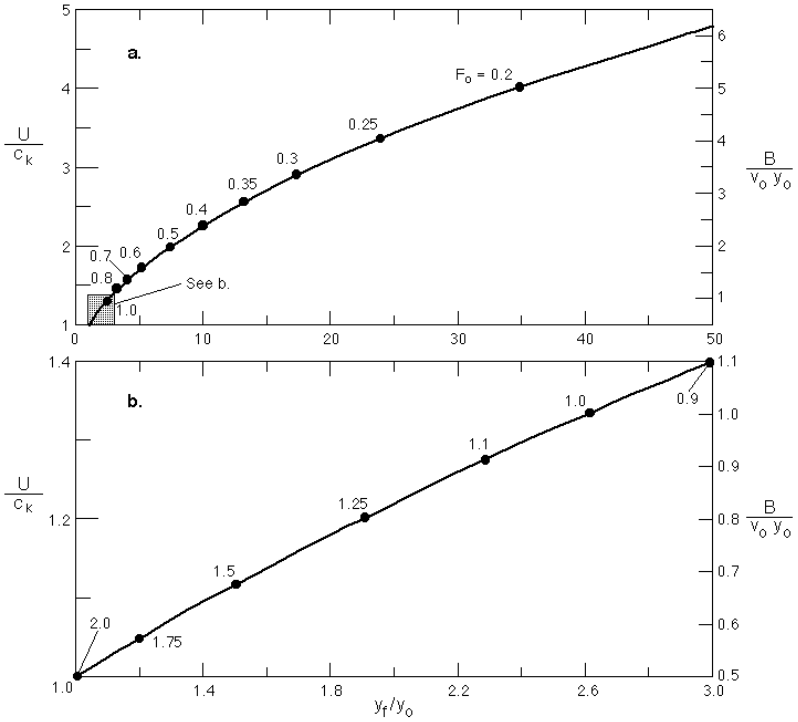

Figure 6. Dimensionless monoclinal profile celerity and overrun discharge as a function of depth ratio. The stable profile range spans a depth ratio range from 1 to an upper bound, indicated by the dots, that decreases as the Froude number increases. Panel b *is an expanded view of the shaded area of panel* a.

For monoclinal–diffusion waves eq 41 has a value of 1, and the deviation from 1 indicates the relative importance of inertia. The same cases analyzed for linear waves are used to depict monoclinal waves, with time deleted from the parameters considered and depth ratio across the wave representing amplitude added. Evaluations of eq 41 for each case are presented in Figure 7 as a function of y_r for selected values of $\tilde{y}$, all with limit $1 - F_0^2/4$ at $y_r = 1$. At low Froude numbers the part of the profile affected by inertia is very close to leading edge (small $\tilde{y}$), and then only when depth ratios are large. Differences between monoclinal and monoclinal–diffusion profiles near the leading edge increase with y_r and F_0. Negative values of eq 41 indicate that the profile point $\tilde{y}$ is located on a shock. Cases I and II have a calculated stability limit of $y_r = 51$, where the dimensionless shock amplitude is smaller than 0.001. In case III with high F_0 much more of the profile is affected by inertia, and larger shocks occur at relatively small depth ratios. Case IV is intermediate between these conditions, and case V is similar to cases I and II.

Monoclinal and monoclinal–diffusion dimensionless depth profiles for case I, presented in Figure 8, are in exact agreement except for the leading edge at $y_r = 50$, where the diffusion solution leads. The front half of these profiles shorten and steepen as y_r increases to 10. At $y_r = 50$ the wave front lengthens, and the steepest portion continues forward to the leading edge. The profile comparisons and trends for case II in Figure 9 are identical to those of case I, except that profile lengths are significantly increased as a result of much higher diffusion. Case III, depicted in Figure 10, has monoclinal and monoclinal–diffusion profiles that progressively separate below a dimensionless depth of about 0.4. The leading edge of the steeper monoclinal profile lags behind that of the diffusion profile. At $y_r = 5$, outside the stable profile range, overrun of the leading edge of the monoclinal profile indicates shock formation up to a dimensionless depth of about 0.1. Case IV in Figure 11 is qualitatively

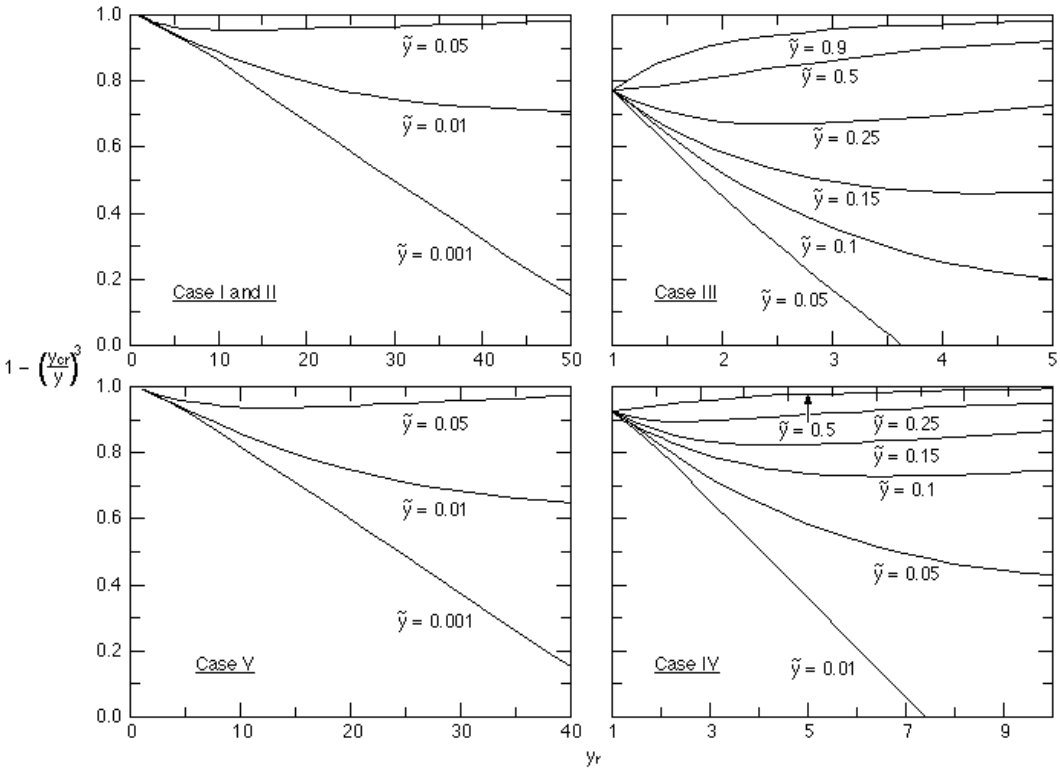

Figure 7. Evaluation of eq 41 as a function of depth ratio for selected dimensionless depths on the monoclinal profile in each case. Note the changes in the depth ratio scale between panels.

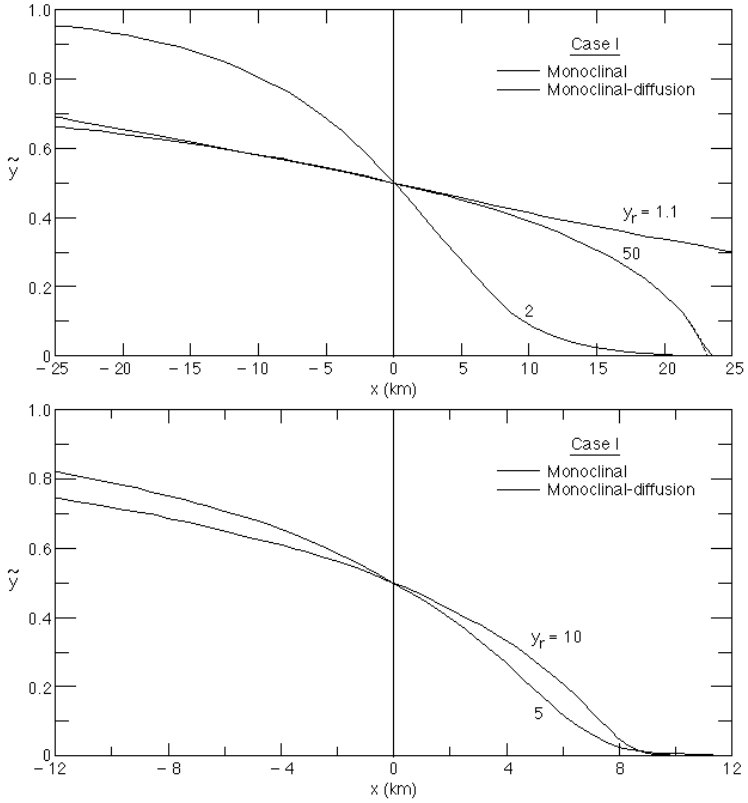

Figure 8. Case I monoclinal and monoclinal–diffusion profiles at two distance scales for depth ratios ranging between 1.1 and 50.

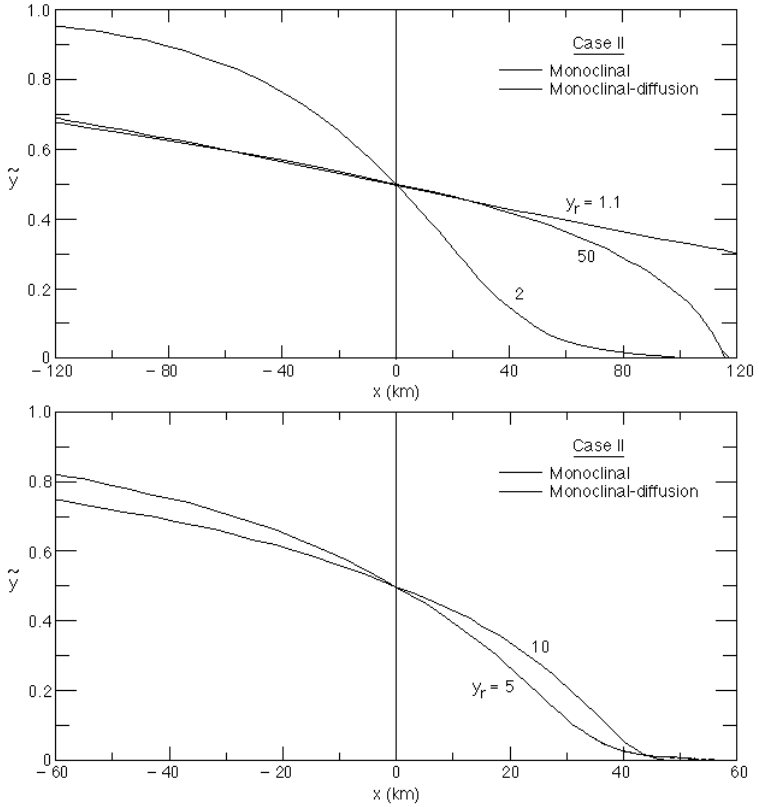

Figure 9. Case II monoclinal and monoclinal–diffusion profiles at two distance scales for depth ratios ranging between 1.1 and 50.

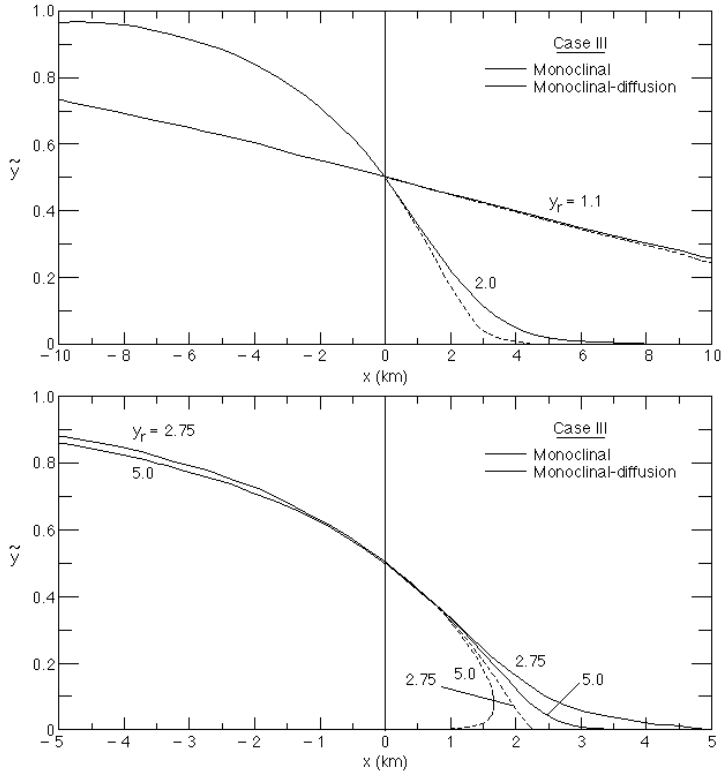

Figure 10. Case III monoclinal and monoclinal–diffusion profiles at two distance scales for depth ratios ranging between 1.1 and 5.

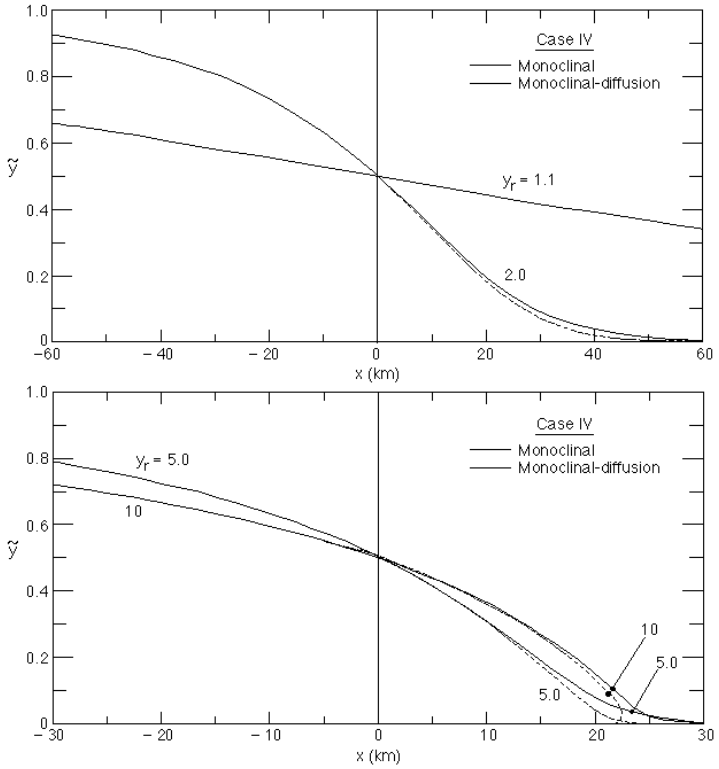

Figure 11. Case IV monoclinal and monoclinal–diffusion profiles at two distance scales for depth ratios ranging between 1.1 and 10.

similar to case III with distance scales substantially increased. At $y_r = 2$ the profiles begin to separate at a dimensionless depth of about 0.3, and an overrun of the leading edge occurs at $y_r = 10$ up to a dimensionless depth of 0.03. Case V, presented in Figure 12, is qualitatively similar to cases I and II except that the largest diffusion coefficient produces the longest profiles of all the cases.

General results from these comparisons are that monoclinal and monoclinal-diffusion profiles agree for all values of y_r with $F_0 \leq 0.2$, and that profile length increases with η or D. At small F_0 the depth ratio needed to produce a shock is large, and the shock height and overrun distance of the leading edge are small. These results agree with the Lighthill and Whitham (1955) contention that dynamic waves are subordinated at "well subcritical" Froude numbers. As F_0 increases the monoclinal waves differ over a larger portion of the profile, shocks occur at smaller depth ratios and their dimensionless amplitudes increase, and for a given η the profile length decreases. General dimensionless monoclinal–diffusion profiles for each depth ratio are given in Figure 13 as a function of $\tilde{x}$, and include the profiles of all cases as indicated by eq 35. Similar dimensionless monoclinal profile plots in Figure 14 are almost as well-behaved, but differences near the leading edge occur for each y_r due to their F_0 dependence.

Steady flow rating curves relate river stage or mean depth at a given location to a unique discharge. The governing equation for linear waves holds with either v or y as the dependent variable, indicating a fixed steady flow rating. In unsteady flow the discharge relating to a given stage generally varies from that for steady flow, depending on the rate of rise or fall of the hydrograph. We will develop and compare dimensionless monoclinal wave and steady flow ratings. Using eq 26, an equation for the monoclinal wave unit discharge can be written in terms of depth and depth ratio as

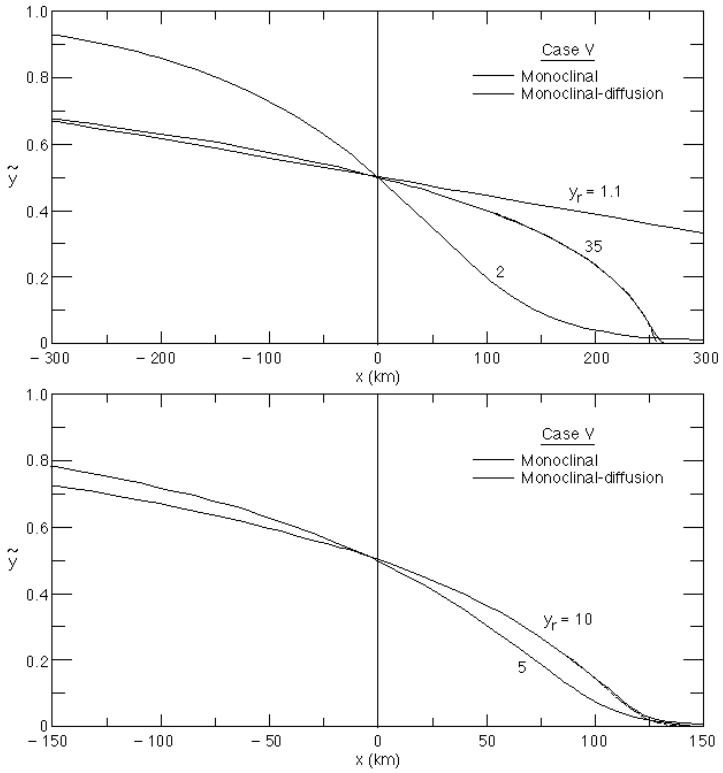

Figure 12. Case V monoclinal and monoclinal–diffusion profiles at two distance scales for depth ratios ranging between 1.1 and 35.

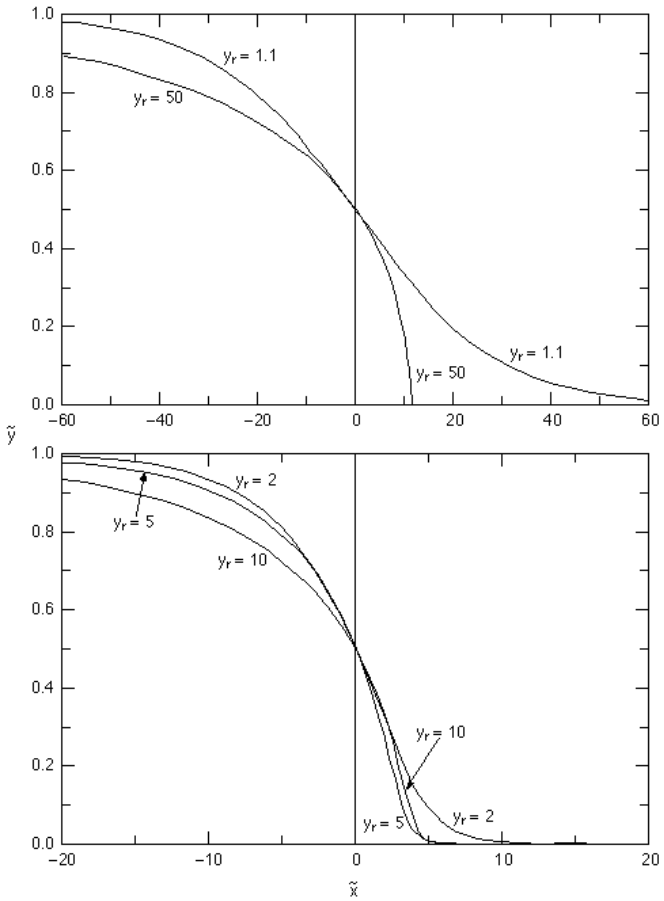

Figure 13. General monoclinal–diffusion profiles at two dimensionless distance scales for depth ratios ranging between 1.1 and 50.

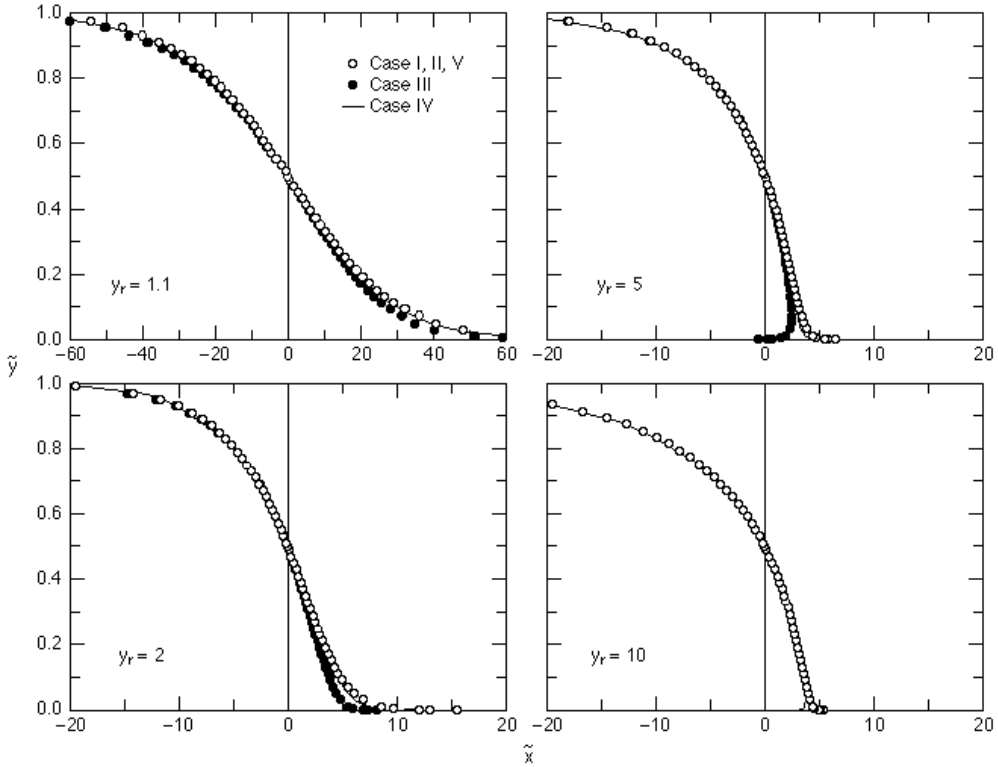

Figure 14. Monoclinal profiles for all cases at two dimensionless distance scales for depth ratios ranging between 1.1 and 10.

$$\frac{q}{q_0} = \frac{vy}{v_0 y_0} = \frac{(y/y_0)(y_r^{3/2} - 1) - y_r(y_r^{1/2} - 1)}{(y_r - 1)}. \tag{42}$$

Defining dimensionless unit discharge with the same form as dimensionless depth, eq 2 becomes

$$\tilde{q} = \tilde{y} \tag{43}$$

independent of the depth ratio. Using the Chezy equation we obtain a corresponding relationship for dimensionless unit discharge in steady flow conditions as a function of depth ratio

$$\tilde{q}_{\text{steady}} = \frac{\left[(y_r - 1)\tilde{y} + 1\right]^{3/2} - 1}{y_r^{3/2} - 1}. \tag{44}$$

In the linear wave limit as y_r approaches 1, the rating curves represented by eq 43 and 44 are identical. These rating curves, given in Figure 15, indicate that for a given dimensionless depth as y_r increases the monoclinal wave unit discharge also increases relative to that for steady flow.

Froude number and energy gradient along a linear wave are unchanged from those of the initial steady flow. Large amplitude monoclinal waves with discharges along the profile that greatly exceed those of steady flow at comparable depths can have significantly larger S_f and F. We define $E \equiv S_f / S_0$, and with the Chezy equation and eq 26 obtain

$$E = \frac{(v/v_0)^2}{y/y_0} = \left(\frac{F}{F_0}\right)^2 = \frac{\left[\left(y_r^{3/2} - 1\right)\tilde{y} + 1\right]^2}{\left[(y_r - 1)\tilde{y} + 1\right]^3}. \tag{45}$$

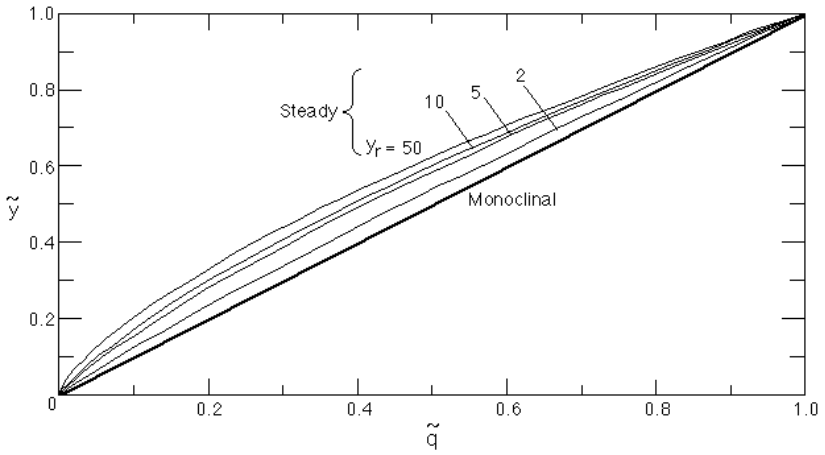

Figure 15. Dimensionless monoclinal and steady state rating curves for depth ratios ranging between 2 and 50.

Figure 16 gives E as a function of $\tilde{y}$ for selected values of y_r. The maximum E increases with y_r and moves from near the midpoint of the profile toward the leading edge. Conversely, Figure 17 gives E as a function of y_r for selected values of $\tilde{y}$. At small y_r the largest E is located near the midpoint of the profile. As y_r increases E approaches a constant starting at the midpoint of the profile and progressing toward the leading edge. At large depth ratios E is inversely proportional to $\tilde{y}$, increasing toward the leading edge.

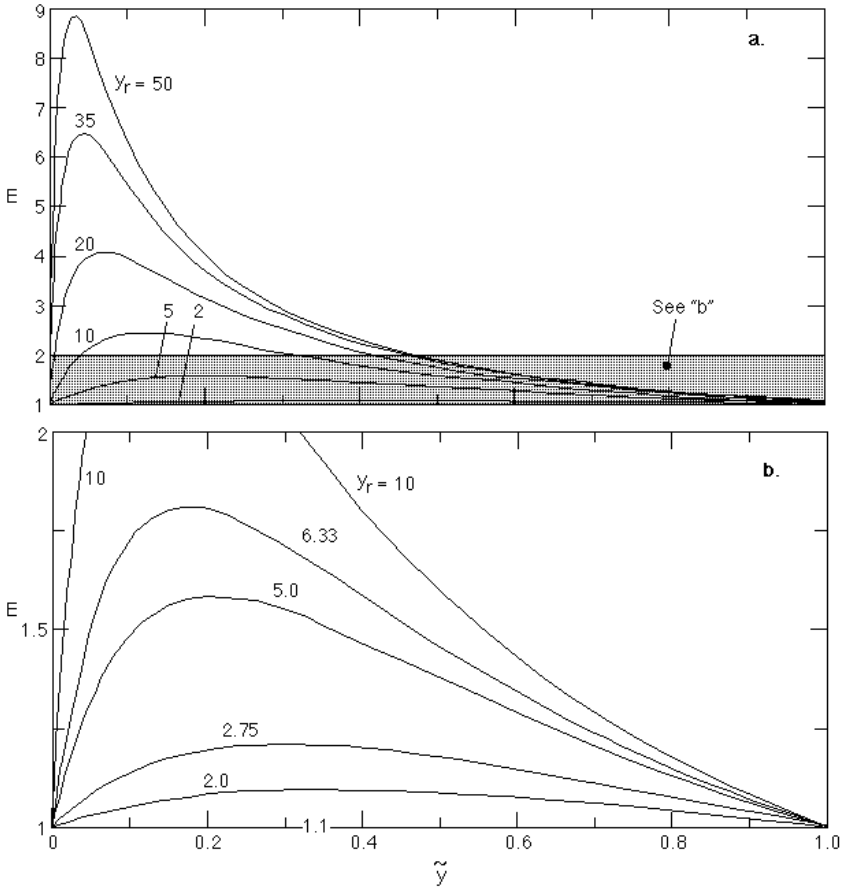

Figure 16. Energy gradient and Froude number parameter E *along the monoclinal wave profile for selected depth ratios. Panel* b *is an expanded view of the shaded area in panel* a.

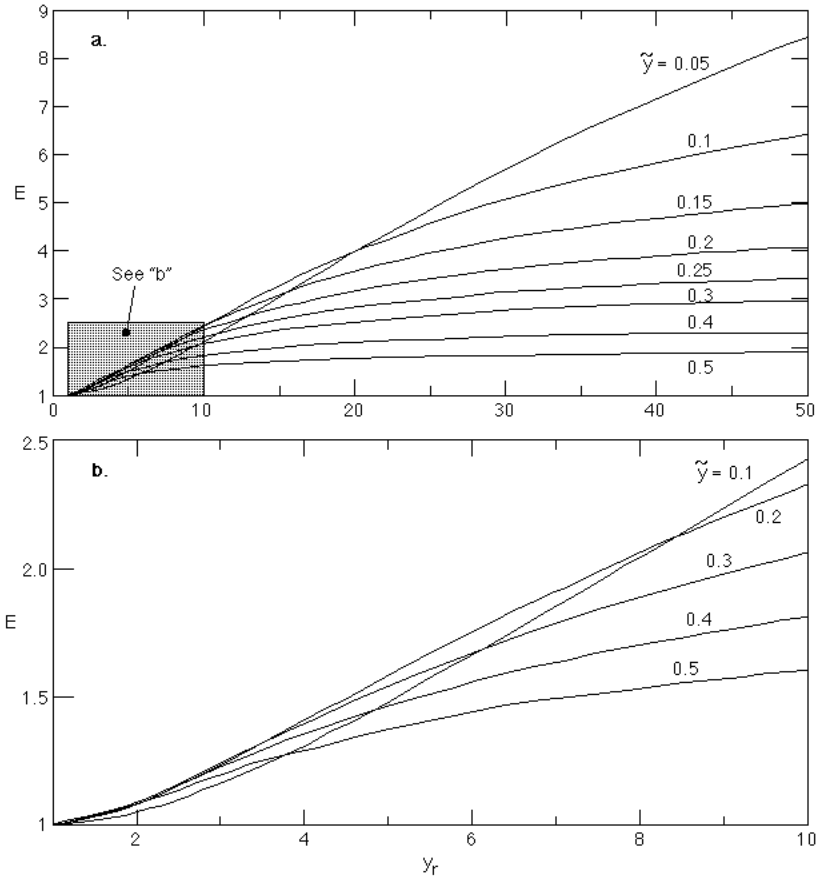

Figure 17. Energy gradient and Froude number parameter E *as a function of depth ratio for selected dimensionless depths along the profile. Panel* b *is an expanded view of the shaded area in panel* a.

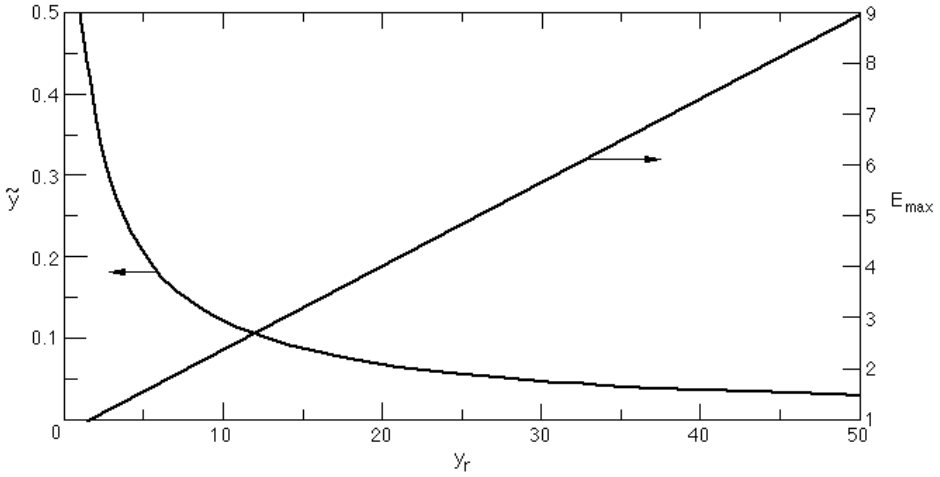

Figure 18. Dimensionless depth and corresponding maximum E *as functions of depth ratio.*

The dimensionless depth corresponding to maximum *E* for a given depth ratio can be obtained by differentiating eq 45 with respect to $\tilde{y}$ and setting the result to zero as

$$\tilde{y} = \frac{2}{y_r - 1} - \frac{3}{y_r^{3/2} - 1}. \tag{46}$$

The maximum E is then obtained by substituting eq 46 into 45 and simplifying

$$E_{\max} = \frac{4}{27} \frac{\left(y_r^{3/2} - 1\right)^3}{y_r \left(y_r - 1\right)^2 \left(y_r^{1/2} - 1\right)}. \tag{47}$$

The location and value of $E_{\max}$ are given in Figure 18. $E_{\max}$ increases nearly linearly over the y_r range, and its location rapidly approaches the leading edge as y_r increases from 1. Both energy gradient and Froude number vary continuously along the monoclinal wave profile, with amplitudes proportional to y_r. Froude numbers that exceed 1 can occur on stable profiles when F_0 is large, as in case III.

CONCLUSIONS

The presence or absence of the inertia terms distinguishes dynamic wave and diffusion wave models of unsteady river flow. Analytical solutions of the linear dynamic wave and diffusion wave equations were compared for a small instantaneous increase from an initial steady, uniform flow condition throughout the channel to a higher steady flow velocity, and depth at the upstream boundary. The comparison used case studies that represented a wide range of flow depth, velocity, channel slope, and wave diffusion coefficient, and spanned the range of subcritical Froude numbers. Analytical solutions were also obtained for nonlinear monoclinal wave and monoclinal–diffusion wave equations, and comparisons were again made using the same case studies with a wide range of wave amplitudes. The linear solution comparisons focused on the evolution of the dynamic wave and diffusion wave profiles with time and distance, while the nonlinear solution comparisons investigated the effects of wave amplitude and persistent inertia.

The linear solution comparisons included the celerity and the trace on the x-t plane of selected points from the wave profile, and the complete dynamic and diffusion profiles at selected times. The initial shock traveled downstream with the dynamic forerunner at c_+, the maximum celerity in subcritical flow. A limitation of the diffusion wave solution is premature replacement of this shock by a profile having a range of point celerities that exceed c_+ near the leading edge. The diffusion wave and dynamic wave profiles remain distinct until after the shock attenuates and their profile celerities converge. In cases where the Froude number approaches 1, this convergence requires a diffusion coefficient corrected for inertia. Points near the leading edge of each profile travel faster than those higher on the profile, causing diffusion. These differences diminish over time and distance, and all dynamic and diffusion profile celerities asymptotically approach that of a kinematic wave. General agreement of the linear diffusion wave and dynamic wave solutions after attenuation of the shock is indicated in all cases by common profile celerities and x-t traces, and by profile covergence with time. The role of the characteristics in the linear solution becomes negligible following shock attenuation at time and distance scales that increase with both η and the Froude number.

The analysis of the nonlinear monoclinal wave solutions linked important inertial effects at large time with increasing Froude number. As F_0 increases corresponding monoclinal and monoclinal–diffusion profiles separate near the leading edge, and these differences increase with wave amplitude. Monoclinal profile instability occurs at higher F_0, but monoclinal–diffusion profiles are always stable. General dimensionless monoclinal–diffusion profiles exist for each depth ratio with distance scaled by y_0 / S_0, but monoclinal profiles deviate from these general profiles at higher F_0. Several effects of wave amplitude on monoclinal waves were also identified. The celerity of a small-amplitude monoclinal wave equals that of a kinematic wave, and it increases continuously from this lower limit with

wave amplitude. The steepness near the front of the monoclinal wave profile and the difference between monoclinal and steady flow or linear wave rating curves both increase as amplitude increases. The energy gradient and Froude number at all points along the profile also increase with wave amplitude, and the location of the maximum shifts continuously toward the leading edge.

LITERATURE CITED

Agsorn, S., and J.C.I. Dooge (1991) Numerical experiments on the monoclinal rising wave. *Journal of Hydrology*, **124**: 293–306.

Carslaw, H.S., and J.C. Jaeger (1959) *Conduction of Heat in Solids*. Oxford: Oxford University Press, 2nd ed., p. 387–388.

Chow, V.T. (1959) *Open Channel Hydraulics*. New York: McGraw-Hill, p. 528–537.

Dooge, J.C.I. (1973) Linear theory of hydrologic systems. USDA Agricultural Research Service, Washington, D.C., Technical Bulletin no.1468.

Dooge, J.C.I., and B.M. Harley (1967) Linear routing in uniform open channels, In *Proceedings of the International Hydrology Symposium, Fort Collins, Colorado, 6–8 September*, vol. 1, p. 57–63.

Ferrick, M.G. (1985) Analysis of river wave types. *Water Resources Research*, **21:** 209–220.

Ferrick, M.G., J. Bilmes, and S.E. Long (1984) Modeling rapidly varied flow in tailwaters. *Water Resources Research*, **20**: 271–289.

Hayami, S. (1951) On the propagation of flood waves. Disaster Prevention Research Institute, Kyoto University, Japan, Bulletin no. 1.

Henderson, F.M. (1966) *Open Channel Flow*. New York: Macmillan Company.

Hunt, B. (1987) A perturbation solution of the flood-routing problem. *Journal of Hydraulic Research*, **25**: 215–234.

Kundzewicz, Z.W., and J.C.I. Dooge (1989) Attenuation and phase shift in linear flood routing. *Hydrological Sciences Journal*, **34**: 21–40.

Lighthill, M.J., and G.B. Whitham (1955) On kinematic waves. I: Flood movement in long rivers. *Proceedings of the Royal Society (London) (A)*, **229**: 281–316.

Mahmood, K., and V. Yevjevich (Ed.) (1975) *Unsteady Flow in Open Channels*. Fort Collins, Colorado: Water Resources Publications, vol. I, p. 29–62.

Mendoza, C. (1995) Discussion of "Identification of reservoir flood-wave models" by V.P. Singh and J. Li. *Journal of Hydraulic Research*, **33**: 420–422.

Menendez, A.N. (1993) The asymptotic wave form for a space-limited perturbation in open channels. *Journal of Hydraulic Research*, **31**: 635–650.

Menendez, A.N., and R. Norscini (1982) Spectrum of shallow water waves: an analysis. *Journal of the Hydraulics Division, ASCE*, **108**: 75–94.

Ponce, V.M., and D.B. Simons (1977) Shallow wave propagation in open channel flow. *Journal of the Hydraulics Division, ASCE*, **103**: 1461–1476.

Ponce, V.M., R.M. Li, and D.B. Simons (1978) Applicability of kinematic and diffusion models. *Journal of the Hydraulics Division, ASCE*, **104**: 353–360.

Press, W.H., S.A. Teukolsky, W.T. Vetterling, and B.P. Flannery (1992) *Numerical Recipes in FORTRAN*. New York: Cambridge University Press, second edition, p. 123–155, 229–233.

Stoker, J.J. (1957) *Water Waves*. New York: Wiley-Interscience, p. 482–509.

Whitham, G.B. (1974) *Linear and Nonlinear waves*. New York: Wiley-Interscience, p. 87–91, 339–350.

Woolhiser, D.A., and J.A. Liggett (1967) Unsteady one-dimensional flow over a plane—The rising hydrograph. *Water Resources Research*, **3**(3), 753–771.

REPORT DOCUMENTATION PAGE

Form Approved
OMB No. 0704-0188

1. AGENCY USE ONLY (Leave blank)	2. REPORT DATE	3. REPORT TYPE AND DATES COVERED
	January 1998	

4. TITLE AND SUBTITLE

Analysis of Linear and Monoclinal River Wave Solutions

5. FUNDING NUMBERS

DA Project DT08
CWIS Project 7VC103

6. AUTHORS

Michael G. Ferrick and Nicholas J. Goodman

7. PERFORMING ORGANIZATION NAME(S) AND ADDRESS(ES)

U.S. Army Cold Regions Research and Engineering Laboratory
72 Lyme Road
Hanover, New Hampshire 03755-1290

8. PERFORMING ORGANIZATION REPORT NUMBER

CRREL Report 98-1

9. SPONSORING/MONITORING AGENCY NAME(S) AND ADDRESS(ES)

Office of the Chief of Engineers
Washington, D.C. 20314-1000

10. SPONSORING/MONITORING AGENCY REPORT NUMBER

11. SUPPLEMENTARY NOTES For conversion of SI units to non-SI units of measurement consult *Standard Practice for Use of the International System of Units (SI)*, ASTM Standard E380-93, published by the American Society for Testing and Materials, 1916 Race St., Philadelphia, Pa. 19103.

12a. DISTRIBUTION/AVAILABILITY STATEMENT

Approved for public release; distribution is unlimited.

Available from NTIS, Springfield, Virginia 22161.

12b. DISTRIBUTION CODE

13. ABSTRACT (*Maximum 200 words*)

Linear dynamic wave and diffusion wave analytical solutions are obtained for a small, abrupt flow increase from an initial to a higher steady flow. Equations for the celerities of points along the wave profiles are developed from the solutions and related to the kinematic wave and dynamic wave celerities. The linear solutions are compared systematically in a series of case studies to evaluate the differences caused by inertia. These comparisons use the celerities of selected profile points, the paths of these points on the *x-t* plane, and complete profiles at selected times, indicating general agreement between the solutions. Initial diffusion wave inaccuracies persist over relatively short time and distance scales that increase with both the wave diffusion coefficient and Froude number. The nonlinear monoclinal wave solution parallels that of the linear dynamic wave but is applicable to arbitrarily large flow increases. As wave amplitude increases the monoclinal rating curve diverges from that for a linear wave, and the maximum Froude number and energy gradient along the profile increase and move toward the leading edge. A monoclinal–diffusion solution is developed for the diffusion wave equations, and dynamic wave–diffusion wave comparisons are made over a range of amplitudes with the same case studies used for linear waves. General dimensionless monoclinal–diffusion profiles exist for each depth ratio across the wave, while corresponding monoclinal wave profiles exhibit minor, case-specific Froude number dependence. Inertial effects on the monoclinal profiles occur near the leading edge, increase with the wave amplitude and Froude number, and are responsible for the differences between the dimensionless profiles.

14. SUBJECT TERMS

Analytical solutions
Diffusion wave
Dynamic wave
Flood routing
Linear waves
Monoclinal waves
River waves
Unsteady flow

15. NUMBER OF PAGES
30

16. PRICE CODE

17. SECURITY CLASSIFICATION OF REPORT	18. SECURITY CLASSIFICATION OF THIS PAGE	19. SECURITY CLASSIFICATION OF ABSTRACT	20. LIMITATION OF ABSTRACT
UNCLASSIFIED	UNCLASSIFIED	UNCLASSIFIED	UL